Research Article | Vol. 29, No. 6 / 15 March 2021 / Optics Express 8880
Optics EXPRESS

Exploration of exciton dynamics in GaTe nanoflakes via temperature- and power-dependent time-resolved photoluminescence spectra

HONGYAN YAN,[1,2] XILONG LIANG,[1,2] SHUAI DONG,[1,2] YU LEI,[3] GUOFENG ZHANG,[1,2] RUIYUN CHEN,[1,2] JIANYONG HU,[1,2] MINGYONG JING,[1,2] SHEN WANG,[3] XINGLIANG SU,[3] CHENGBING QIN,[1,2,4] LIANTUAN XIAO,[1,2,5] AND SUOTANG JIA[1,2]

[1]*State Key Laboratory of Quantum Optics and Quantum Optics Devices, Institute of Laser Spectroscopy, Shanxi University, Taiyuan, Shanxi 030006, China*
[2]*Collaborative Innovation Center of Extreme Optics, Shanxi University, Taiyuan, Shanxi 030006, China*
[3]*College of Physics and Electronics Engineering, Shanxi University, Taiyuan, Shanxi 030006, China*
[4]*chbqin@sxu.edu.cn*
[5]*xlt@sxu.edu.cn*

Abstract: GaTe nanoflakes have been receiving much research attention recently due to their applications in optoelectronic devices, such as anisotropic non-volatile memory, solar cells, and high-sensitivity photodetectors from the ultraviolet to the visible region. Further applications, however, have been impeded due to the limited understanding of their exciton dynamics. In this work we perform temperature- and power-dependent time-resolved photoluminescence (PL) spectra to comprehensively investigate the exciton dynamics of GaTe nanoflakes. Temperature-dependent PL measurements manifest that spectral profiles of GaTe nanoflakes change dramatically from cryogenic to room temperature, where the bound exciton and donor-to-acceptor pair transition normally disappear above 100 K, while the charged exciton survives to room temperature. The lifetimes of these excitons and their evolution *vs* temperature have been uncovered by time-resolved PL spectra. Further measurements reveal the entirely different power-dependent exciton behaviors of GaTe nanoflakes between room and cryogenic temperatures. The underlying mechanisms have been proposed to explore the sophisticated exciton dynamics within GaTe nanoflakes. Our results offer a more thorough understanding of the exciton dynamics of GaTe nanoflakes, enabling further progress in engineering GaTe-based applications, such as photodetectors, light-emitting diodes, and nanoelectronics.

1. Introduction

Very recently, two-dimensional III-VI group layered materials with the chemical formula of MX (M = In, Ga; X = S, Se, Te) have received considerable attention [1,2], due to their unique features, such as wide light absorption range [3], suitable energy band gaps [4], large nonlinear coefficient [5], high performance in carrier mobility and on/off ratio [6], as well as good light responsiveness in visible-ultraviolet light [7]. These superiorities make them tremendous application prospects in photovoltaic devices [8], optoelectronic devices [9], nonlinear optics [10], and microelectronics [6]. Furthermore, compared to molybdenum and tungsten chalcogenides emitting light efficiently only in films with a single unit cell thickness [11], III-VI group materials are bright light emitters in a range of thicknesses [12]. This may relax the stringent fabrication requirements and show more competition for novel heterostructured devices in light-emitting diodes.

#418749 https://doi.org/10.1364/OE.418749
Journal © 2021 Received 4 Jan 2021; revised 19 Feb 2021; accepted 27 Feb 2021; published 8 Mar 2021

Optics EXPRESS

Gallium telluride (GaTe) is one kind of III-VI group layered semiconductor material. The main components of the III-VI group, including GaS, GaSe, InS, and InSe, are crystallizing in a four-sheet sublayer stacking pattern (X-M-M-X) with each sublayer of hexagonal structure. Different from these materials, bulk GaTe appears as a distorted form of the MX structures, belonging to the monoclinic lattice system with a space group of C_{2h}^3 [13,14]. In this case, two-thirds of Ga-Ga bonds are perpendicular to the layer plane and one-third are almost in the layer plane [15]. Interestingly, the newest study demonstrated the thickness-induced structural phase transformation of layered GaTe between monoclinic and hexagonal structures [16]. Furthermore, Ho group also reported the coexistence of monoclinic and hexagonal phases in multilayered GaTe, which emerged two-color photoluminescence (PL) emission [17]. This phenomenon can be partly derived from the 2H (two-layer hexagonal) crystal structure of $GaSe_{1-x}S_x$ series solids [18]. Consequently, the complicated crystal structure of GaTe emerges unique optical and electrical properties, as compared with other III-IV layered materials. Taking anisotropy as an example, electrical conductivity anisotropy between x and y directions of GaTe nanoflakes can be gate tuned from several folds to over 10^3, yielding an anisotropic non-volatile memory behavior in GaTe nanoflakes [6]. Similarly, only x-polarized transition is allowed in the band edge of multilayer GaTe, rather than both x- and y-polarized transitions coexisting in the other MX layered semiconductors [19]. On the other aspect, GaTe nanoflakes have a direct bandgap of about 1.67 eV, making GaTe extremely valuable in the fields of optoelectronic devices [7], radiation detectors [20], and solar cells [21]. The photodetectors based on GaTe nanoflakes exhibit a remarkable photoresponsivity better than 10^4 A/W and response speed faster than 6 ms, which are better than that of graphene, MoS_2, and other layered materials. Theoretical calculations predict that GaTe-graphene heterostructures can combine the intense response to visible light as well as the high energy radiation photoabsorption of GaTe, with the ballistic transport properties of graphene, to extended applications in solar cells and radiation detectors [9]. Although GaTe nanoflakes have been widely used in photodetectors, comprehensive investigations on exciton dynamics of GaTe nanoflakes are still limited, which will be helpful to improve the photoresponsivity and sensitivity of the optoelectronic devices.

In this work, we perform temperature- and power-dependent time-resolved PL spectra to reveal the exciton dynamics of GaTe nanoflakes. We attribute the asymmetric spectra profiles of GaTe nanoflakes at room temperature to the combination of neutral excitons (X^0) and charged excitons (X^T), with the dissociation energy of X^T about 13 meV. PL spectra under cryogenic conditions have been attributed to the combination of donor-to-acceptor transition (X^{DAP}), shallow-acceptor-bound exciton (X^{SAB}), and X^T, where both X^{DAP} and X^{SAB} rapidly disappear with the increase of temperature and quickly saturate with the increase of excitation power. The lifetimes of X^{DAP} and X^{SAB} are determined to be around 100 ns and 10 ns, which shorten with the increase in temperature. The underlying mechanisms have been proposed to explore the sophisticated exciton dynamics within GaTe nanoflakes.

2. Experiment

2.1. Sample preparation and characterization

GaTe nanoflakes were prepared by mechanical exfoliation from bulk crystal, purchasing from SxiCarbon Technology (Shenzhen), and then transferred on a SiO_2/Si substrate. The morphology of GaTe nanoflakes was characterized by optical microscope (OLYMPUS TH4-200) and atomic force microscope (AFM, Flex-Axi). And the Raman spectra were recoeded by a commercial Raman spectrometer (LabRAM HR, Horiba) using the 532 nm laser excitation.

Optics EXPRESS

2.2. Optical setup

The optical experiments at both room temperature and cryogenic conditions were performed by using a home-built scanning confocal microscope. The experimental schematic has been illustrated in the Appendix (Fig. 5). Particularly, a 532 nm continuum-wave laser (CW, MSL-FN-532, CNI) was used to carry out PL spectra. A pulse laser at the wavelength of 532 nm with a pulse width of about 100 ps was used to perform the time-resolved PL spectra, at the repetition frequency of 5 MHz (Sc-Pro, Yangtze Soton Laser). The laser beam was focused by an objective (60×, NA=0.82, NIRLT-APO, Attocube) with the lateral dimension of the focal spot of about 600 nm. The GaTe nanoflakes were mounted in a cryogenic vacuum chamber (Montana Instruments), of which the temperature can be varied from 4 K to room temperature. PL imaging of GaTe nanoflakes was created through a 4-*f* system with a fast-steering scanner (FSM-300-M-03, Newport). PL intensity and its spectrum were synchronously recorded, by using a single-photon detector (SPCM-AQR-15, PerkinElmer) and a monochromator equipped with a cooled charge-coupled device (CCD, DU920P, Andor), respectively.

3. Results and discussion

Abundant GaTe nanoflakes with the thickness ranging from several to hundreds of nanometers were prepared by mechanical exfoliation and transferred on a SiO_2/Si substrate. We find that PL spectra of ultrathin GaTe nanoflakes (less than 20 nm) show dramatic variations from sample to sample at cryogenic conditions, as they are most likely related to crystal defects and degradation [12]. Further works are needed to clarify this phenomenon. We have confirmed that GaTe nanoflakes with a thickness larger than 30 nm emerge similar exciton behaviors. Here we present a typical result of a GaTe nanoflake with a thickness of about 100 nm. Figure 1(a) shows the optical imaging of the GaTe nanoflake, the relative homogenous contrast color indicates that the basal plane of GaTe is flat and uniform. The thickness of the nanoflake has been explored by AFM characterization, as shown in Fig. 1(b). The height of the cross line has been presented in the inset. Raman spectroscopy were further used to characterize the sample, as shown in Fig. 1(c). The 520 cm^{-1} phonon mode from the Si substrate was used for calibration. The Raman peaks at 105, 111, 159, 173, 205, 266, and 281 cm^{-1} can be assigned to the representative vibration modes of the monoclinic phase of GaTe crystal, consisting reasonably well with previous works [22]. Figure 1(d) presents PL spectra of the GaTe nanoflake at room temperature. To our knowledge, GaTe materials with different thicknesses normally emerge asymmetric spectral profiles [19,23,24], however, a clear explanation is still lacking. The PL spectra can be reasonably fitted by two Lorentzian curves. Thus, two possibilities might be responsible for the asymmetric shape. In one aspect, we can assign the two peaks to the neutral exciton (X^0) and charged exciton (trion, X^T), as the mature treatment in transition metal dichalcogenides [25,26]. X^T possibly results from unintentional doping. In another aspect, the two peaks can be attributed to the optical transition of the monoclinic and hexagonal phase of GaTe nanoflakes, inspired by the very recent works concerning on phase transformation of GaTe and PL spectra of GaSe [16,27]. However, further experimental and theoretical considerations about the later assignment are still under investigation. Here, we tentatively attribute the two components to X^0 and X^T.

We firstly perform the temperature-dependent PL spectra and time-resolved PL measurements of GaTe nanoflakes, which can provide important information on exciton dynamics of semiconductor materials. Figure 2(a) presents the evolution of PL spectra as a function of temperature. We can find that at cryogenic conditions (ranging from 4 K to 90 K), GaTe emerges multi-peaks with the energies of about 1.757 eV, 1.701 eV, and 1.594 eV [as shown in Fig. 2(b)]. These results are somewhat different from previous works about GaTe bulk crystal [15,28,29] or recent work about ribbon-like multilayer GaTe [19]. The low-energy peak with broadening feature can be attributed to the donor-acceptor pair transition (X^{DAP}), the middle one can be assigned to the shallow-acceptor-bound exciton (X^{SAB}), as suggested by Ho et al. [19]. Based on the

Optics EXPRESS

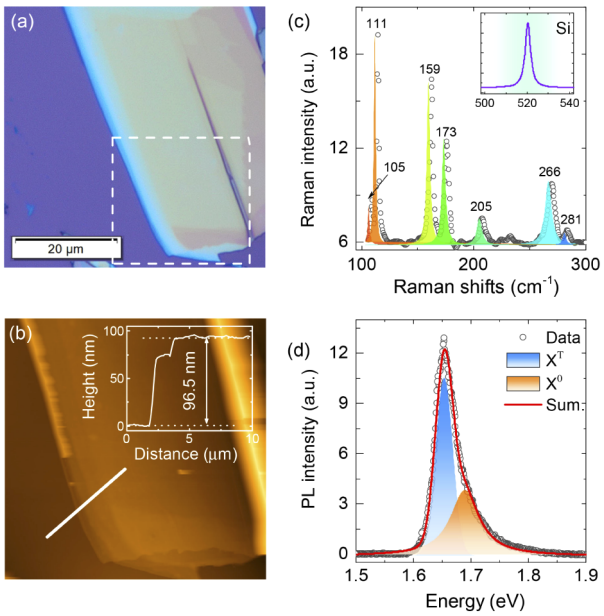

Fig. 1. Characterizations of the GaTe nanoflakes. Optical image (a) and atomic force microscopy (AFM) image (b) of the GaTe nanoflake prepared by mechanical exfoliation. The dashed square in (a) highlights the scanning region of AFM. The inset in (b) is the height profile of the selected line. (c) Raman spectra of the GaTe nanoflake excited by a 532 nm continue-wave laser. Raman shifts of seven main peaks have been marked. (d) Photoluminescence (PL) spectra of the GaTe nanoflake, which is fit to two Lorentzian curves. The component with the blue shadow is assigned to trion emission (X^T), and the other to neutral exciton emission (X^0).

assignment at room temperature mentioned above, we suggest the high-energy peak to X^T, rather than free exciton (X^0). Otherwise, the new-formed peak at the high-energy tail is intricate and unassigned. As the temperature increases from 4 K to room temperature, the PL intensity of both X^{DAP} and X^{SAB} decays rapidly and disappears at about 100 K, due to thermal ionization. On the other aspect, even though the PL intensity of X^T decreases, it still survives at room temperature. The redshift of X^T peak energy can be well fitted by Varshni semiempirical relationship $E(T) = E(0) - \alpha T^2/(\beta + T)$, yielding the transition energy $E(0)$ to be 1.765(6) eV, the strength of exciton-phonon interaction α to be 0.5(2) meV/K, and the parameter β to be 189(26) K, respectively. The values of α and β are agreement rationally good with the relevant works [19], while the transition energy is slight redshift, as compared with the reported value of ~1.79 eV [28,29]. Two possible reasons may be responsible for the energy variation. One is the difference in the thickness and quality of GaTe materials, the other is the diversity of the trion dissociation energy ΔE (the energy difference between X^0 and X^T). Beyond the redshift of peak energy, the full width at half maximum (FWHM) of X^T exhibits significantly broadening with the increase of temperature, which can attribute to the increasing probability of collision between exciton and longitudinal optical phonons [30].

Figure 2(d) presents the time-resolved PL intensity as a function of sample temperature. Notably, when the temperature is higher than 110 K, PL traces of the GaTe nanoflake are close to instrument response function (IRF), while for the traces below 110 K, PL decays can be fitted with a triple exponential function $I(t) = \sum_{i=1}^{3} A_i \cdot e^{-t/\tau_i}$, as the solid lines shown in Fig. 2(d). These behaviors are in agreement favorable with the evolution of their spectra under different

Optics EXPRESS

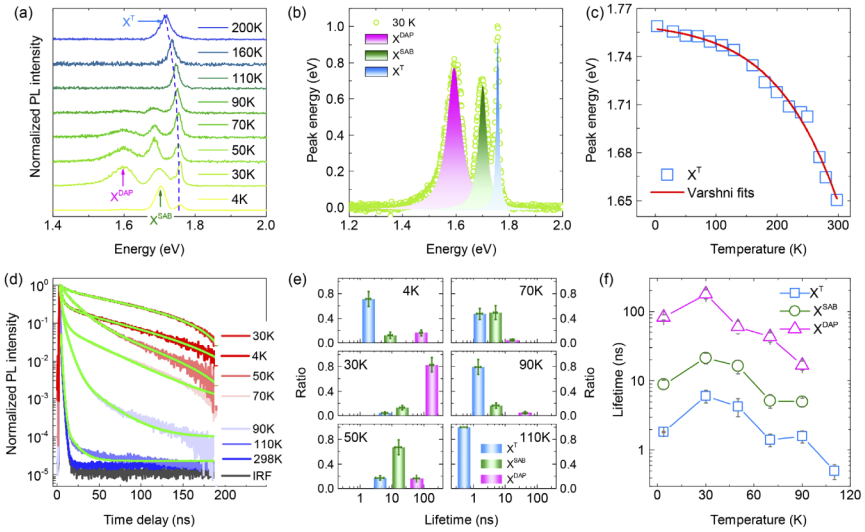

Fig. 2. Temperature-dependent PL spectra and time-resolved PL measurements of GaTe nanoflakes. (a) PL spectra measured at different temperatures. The assignment (X^{DAP}, X^{SAB}, and X^{T}) of PL peaks have been labeled in the figure, the dashed line indicates the redshift of X^{T}. (b) Representative analysis of PL spectra (30 K) using three Lorentzian curves. (c) Peak energy of X^{T} as a function of temperature, the solid line is the Varshni fit. (d) Time-resolved PL decay curves obtained at different temperatures; the solid lines are the triple exponential fits. (e) and (f) are the fitted lifetimes of three components and their relative ratios as a function of temperature.

temperatures. The fitted lifetimes of each component and their relative ratios have been listed in Table 1 and Fig. 2(e). We can find that both lifetimes and their ratios [Fig. 2(e)] show dramatic change. Taking the component with the shortest lifetime as an example, its lifetime changes from a few nanoseconds to sub-nanoseconds and the ratio varies from 4% (30 K) to 100% (110 K). These results hint the complicated exciton dynamics of GaTe nanoflakes under different temperatures. Combining the evolution of PL spectra and lifetimes, the short value (between sub- to several nanoseconds) can be attributed to the lifetime of X^{T}, the middle one (in the region of 5 ns and 21 ns) to that of X^{SAB}, and the long lifetime (16 ns to 177 ns) to that of X^{DAP}. Although time-resolved PL of the GaTe nanoflake presents sophisticated behaviors, their lifetimes become shorter gradually with the increasing temperature, originating from the enhanced interaction between the exciton with the longitudinal optical phonons.

Table 1. Fitting parameters of time-resolved PL spectra under different temperatures.

Temp.	τ_1 (ns)	A_1	τ_2 (ns)	A_2	τ_3 (ns)	A_3	τ_{av} (ns)
4 K	1.83(3)	0.718(12)	8.87(136)	0.121(54)	82.17(654)	0.161(46)	15.64
30 K	6.02(125)	0.041(21)	21.14(354)	0.129(32)	177.22(2536)	0.830(120)	150.11
50 K	4.27(123)	0.168(35)	16.26(365)	0.673(120)	60.26(1254)	0.159(57)	21.25
70 K	1.41(30)	0.792(120)	5.17(117)	0.162(45)	42.62(667)	0.046(23)	3.91
90 K	1.58(32)	0.469(89)	4.95(68)	0.488(110)	16.64(235)	0.042(16)	3.86
110 K							0.50(12)

The excitation power dependence of PL spectra can provide further insights into the physical origins of the corresponding PL peaks and the potential many-body effect within the materials.

Optics EXPRESS

Figure 3 depicts PL spectra of the GaTe nanoflake at room temperature under different excitation powers. To our surprise, PL intensity displays a tendency to saturate rapidly and even emerges slight quenching behavior [the inset in Fig. 3(a)], indicating the presence of exciton-exciton annihilation (EEA) under relative high-power excitation. Furthermore, the saturation of X^T is faster than that of X^0 [Fig. 3(d)], indicating the limited free charges within this GaTe nanoflake. Further experiments with high temporal resolution (such as transient absorption or reflective spectrum [31–33]) are needed to explore the EEA and many-body effect within GaTe nanoflakes. On the other hand, beyond expected power-induced broadening [Fig. 3(c)], the change in the PL spectral profiles can be ignored. Thus, PL spectra are deconvoluted by two peaks [as processing in Fig. 1(d)] for the full power region and assigned to X^0 and X^T, respectively. We can find that under the low excitation power, the energy peaks of X^0 and X^T, as well as their difference ΔE, almost stand at a plateau level. In this case, the trion dissociation energy ΔE can be determined to be about 13 meV, close to the reported thermal energy of bound exciton within GaTe nanoflakes [19]. Under the high excitation power, X^0 emerges dramatic blueshift, while X^T presents redshift, as shown in Fig. 3(b). These phenomena might originate from the combination of the EEA effect and band-structure renormalizations under high carrier concentrations [34].

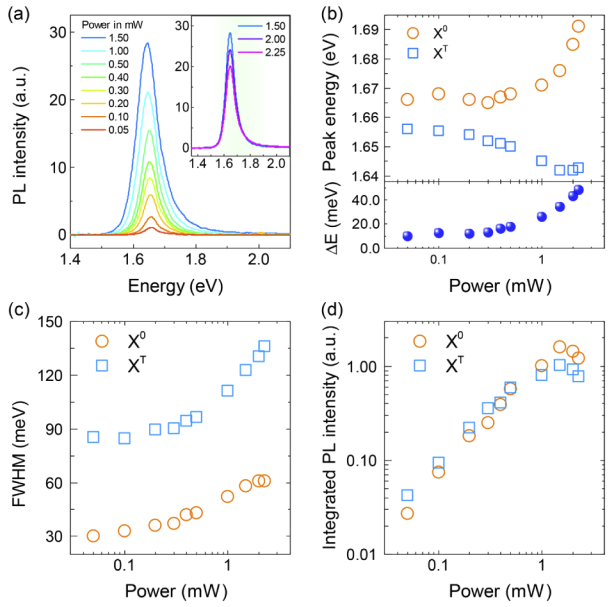

Fig. 3. Excitation power-dependent PL spectra of the GaTe nanoflake at room temperature. (a) Evolution of PL spectra as a function of excitation power. (b) Peak energies, (c) full width at half maximum (FWHM), and (d) the integrated PL intensities of X^0 and X^T as a function of excitation power. The bottom panel in (b) presents the trion dissociation energy ΔE varied as the excitation power.

Excitation power-dependent PL spectra of the GaTe nanoflake under the temperature of 4 K are more complicated, emerging significant change in their spectra together with PL intensity, as shown in Fig. 4 (PL spectra in the logarithmic plot can be found in the Appendix, Fig. 6). At low power excitation, GaTe presents three main peaks, which can be assigned to X^T, X^{SAB}, and X^{DAP} [the inset of Fig. 4(a)], as we discussed above. Since X^{SAB} and X^{DAP} are associated with excitons bound to the donor or acceptor levels, their PL intensities are expected to saturate at high excitation power when these levels are fully populated with excitons. Consistent with this expectation, both X^{SAB} and X^{DAP} exhibit a sub-linear power dependence and saturate rapidly. In contrast, the PL intensity of X^T almost scales linearly (with the power exponent of 1.07),

Optics EXPRESS

without a significant sign of saturation in this power region. As a result, the overall PL spectra are mostly dominated by X^{SAB} and X^{DAP} at low power excitation, while X^{T} becomes observable and predominant at high excitation intensities, as the spectral weight shown in Fig. 4(d). The solid lines shown in Figs. 4(c) and 4(d) are empirical fitting curves, with the formulas and parameters listed in Tables 2 and 3. During the evolution of PL intensity, their peak energies also manifest considerable change, as depicted in Fig. 4(b). With the increase of excitation power, both X^{T} and X^{DAP} present persistent redshift, coinciding with the variation of X^{T} at room temperature [Fig. 3(b)]. Whereas the evolution of X^{SAB} is sophisticated, redshift at relatively low power excitation and then recovering to the initial value when the power intensities are further increased.

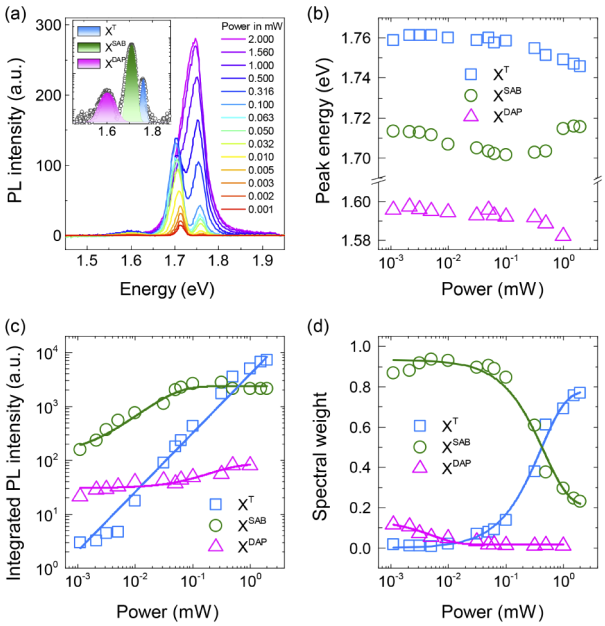

Fig. 4. Excitation power-dependent PL spectra of the GaTe nanoflake at 4 K (a) Evolution of PL spectra as a function of excitation power. The inset depicts the deconvolution via three Lorentzian curves and their assignments. (b) Peak energies, (c) the integrated PL intensities, and (d) the spectral weight of X^{T}, X^{SAB}, and X^{DAP} as a function of excitation power. The solid lines in (c) and (d) are the empirical fits with the corresponding formulas and parameters listed in Tables 2 and 3.

Table 2. Power-dependent parameters of X^{SAB} and X^{DAP} at 4 K.

Equation	$y_i = y_0 + A_i \times e^{x_i/P_i}$							
Terms	X^{SAB}				X^{DAP}			
Intensity	I_0	A	P	R^2	I_0	A	P	R^2
	2355(108)	−2247(174)	−0.031(8)	0.928	84(8)	−53(7)	−0.29(11)	0.898
Weight	W	A	P	R^2	W	A	P	R^2
	0.21(4)	0.73(4)	−4.7(8)	0.975	0.018(3)	0.12(1)	−0.005(1)	0.942

Optics EXPRESS

Table 3. Power-dependent parameters of X^T at 4 K.

Terms	Intensity			Spectral weight			
Equation	$y = a \times x^b$			$y_i = y_0 + A_i \times e^{x_i/P_i}$			
Values	a	b	R^2	I_0	A	P	R^2
	3942(230)	1.1(1)	0.937	0.78(2)	−0.78(2)	−0.41(4)	0.993

4. Conclusion

In conclusion, we perform temperature- and power-dependent PL spectra of GaTe nanoflakes to investigate their exciton dynamics. By analyzing the temperature-dependent measurements, we propose that the charged exciton (X^T), donor-acceptor pair transition (X^{DAP}), and shallow-acceptor-bound exciton (X^{SAB}) dominate PL spectra of GaTe nanoflakes at cryogenic conditions under low power excitation, while PL spectra at room temperature are mainly attributed to X^T and neutral exciton (X^0). The dissociation energy of X^T is extracted to be around 13 meV at low power excitation. The lifetimes of X^T, X^{DAP}, and X^{SAB} and their evolution have been demonstrated by time-resolved PL traces. Power-dependent measurements reveal the sophisticated behaviors of excitons within GaTe nanoflakes. The overall PL intensity at room temperature manifests saturation rapidly and even quenches slightly at high power excitation. While only X^{DAP} and X^{SAB} at cryogenic conditions tend to saturate with the increase of power intensity, X^T emerges a linear power dependence. The exploration of exciton behaviors within GaTe nanoflakes has been proposed and discussed. The presented results offer a comprehensive insight into the exciton dynamics of GaTe nanoflakes which may aid further applications in GaTe based photodetectors, light-emitting diodes, and solar cells.

Appendix

Note: The time-resolved PL spectra were fitted via triple exponential function:

$$I(t) = \sum_{i=1}^{3} A_i \cdot e^{-t/\tau_i} \tag{1}$$

τ_1, τ_2, and τ_3 are the lifetimes of X^T, X^{SAB}, and X^{DAP}. The values in the brackets represent the corresponding standard derivations.

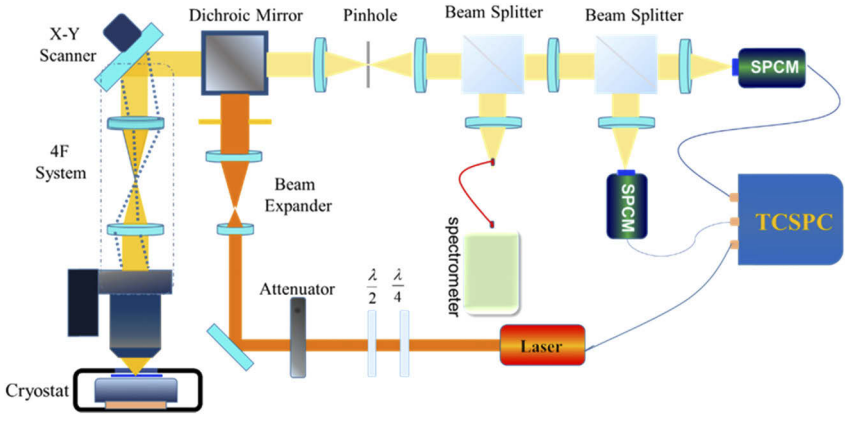

Fig. 5. Confocal fluorescence microscopy setup with time-tagged equipment.

Optics EXPRESS

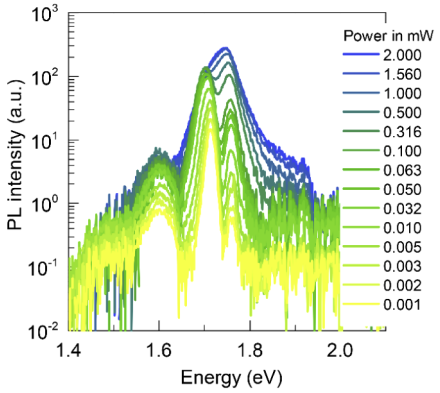

Fig. 6. Evolution of PL spectra as a function of excitation power at 4 K in a logarithmic plot.

Funding. National Key Research and Development Program of China (2017YFA0304203); National Natural Science Foundation of China (61875109, 62011530047, 62075120, 62075122, 91950109); Natural Science Foundation of Shanxi Province (201901D111010(ZD)); PCSIRT (IRT_17R70); Higher Education Discipline Innovation Project (D18001); PTIT; 1331KSC; Postgraduate Education Innovation Project of Shanxi Province (2019SY052, 2020BY022).

Acknowledgments. C. Q., and H. Y. designed and supervised the experiments. H. Y., X. L., and S. D. carried out the optical experiments. Y. L., S. W., and X. S. prepared and characterized the sample. G. Z., M. J., and J. H. contributed to the data analysis. R. C., and S. J. was responsible for instruments managing. H. Y., C. Q., and X. L. wrote the manuscript. All authors commented on the manuscript.

Disclosures. The authors declare no competing interests.

Data availability. Data underlying the results presented in this paper are not publicly available at this time but may be obtained from the authors upon reasonable request.

References

1. K. Xu, L. Yin, Y. Huang, T. A. Shifa, J. Chu, F. Wang, R. Cheng, Z. Wang, and J. He, "Synthesis, properties and applications of 2D layered M(III)X(VI) (M = Ga, In; X = S, Se, Te) materials," Nanoscale **8**(38), 16802–16818 (2016).
2. X. Q. Tian, J. Y. Duan, M. Kiani, Y. D. Wei, N. Feng, Z. R. Gong, X. R. Wang, Y. Du, and B. I. Yakobson, "Hexagonal layered group iv-vi semiconductors and derivatives: Fresh blood of the 2D family," Nanoscale **12**(25), 13450–13459 (2020).
3. D. J. Terry, V. Zólyomi, M. Hamer, A. V. Tyurnina, D. G. Hopkinson, A. M. Rakowski, S. J. Magorrian, N. Clark, Y. M. Andreev, O. Kazakova, K. Novoselov, S. J. Haigh, V. I. Fal'ko, and R. Gorbachev, "Infrared-to-violet tunable optical activity in atomic films of gase, inse, and their heterostructures," 2D Mater. **5**(4), 041009 (2018).
4. C. S. Jung, F. Shojaei, K. Park, J. Y. Oh, H. S. Im, D. M. Jang, J. Park, and H. S. Kang, "Red-to-ultraviolet emission tuning of two-dimensional gallium sulfide/selenide," ACS Nano **9**(10), 9585–9593 (2015).
5. B. Jiang, Z. Hao, Y. Ji, Y. Hou, R. Yi, D. Mao, X. Gan, and J. Zhao, "High-efficiency second-order nonlinear processes in an optical microfibre assisted by few-layer gase," Light: Sci. Appl. **9**(1), 63 (2020).
6. H. Wang, M. L. Chen, M. Zhu, Y. Wang, B. Dong, X. Sun, X. Zhang, S. Cao, X. Li, J. Huang, L. Zhang, W. Liu, D. Sun, Y. Ye, K. Song, J. Wang, Y. Han, T. Yang, H. Guo, C. Qin, L. Xiao, J. Zhang, J. Chen, Z. Han, and Z. Zhang, "Gate tunable giant anisotropic resistance in ultra-thin gate," Nat. Commun. **10**(1), 2302 (2019).
7. F. C. Liu, H. Shimotani, H. Shang, T. Kanagasekaran, V. Zolyomi, N. Drummond, V. I. Fal'ko, and K. Tanigaki, "High-sensitivity photodetectors based on multilayer gate flakes," ACS Nano **8**(1), 752–760 (2014).
8. S. S. Abed Al- Abbas, M. K. Muhsin, and H. R. Jappor, "Tunable optical and electronic properties of gallium telluride monolayer for photovoltaic absorbers and ultraviolet detectors," Chem. Phys. Lett. **713**, 46–51 (2018).
9. J. A. Olmos-Asar, C. R. Leão, and A. Fazzio, "Novel III-Te–graphene van der waals heterojunctions for optoelectronic devices," RSC Adv. **7**(51), 32383–32390 (2017).
10. W. Jie, X. Chen, D. Li, L. Xie, Y. Y. Hui, S. P. Lau, X. Cui, and J. Hao, "Layer-dependent nonlinear optical properties and stability of non-centrosymmetric modification in few-layer gase sheets," Angew. Chem. Int. Ed. **54**(4), 1185–1189 (2015).
11. K. F. Mak, C. Lee, J. Hone, J. Shan, and T. F. Heinz, "Atomically thin MoS_2: A new direct-gap semiconductor," Phys. Rev. Lett. **105**(13), 136805 (2010).

Optics EXPRESS

12. O. D. Pozo-Zamudio, S. Schwarz, M. Sich, I. A. Akimov, M. Bayer, R. C. Schofield, E. A. Chekhovich, B. J. Robinson, N. D. Kay, O. V. Kolosov, A. I. Dmitriev, G. V. Lashkarev, D. N. Borisenko, N. N. Kolesnikov, and A. I. Tartakovskii, "Photoluminescence of two-dimensional GaTe and GaSe films," 2D Mater. **2**(3), 035010 (2015).
13. D. T. Do, S. D. Mahanti, and C. W. Lai, "Spin splitting in 2D monochalcogenide semiconductors," Sci. Rep. **5**(1), 17044 (2015).
14. C. Wei, X. Chen, D. Li, H. Su, H. He, and J. F. Dai, "Bound exciton and free exciton states in GaSe thin slab," Sci. Rep. **6**(1), 33890 (2016).
15. A. Zubiaga, J. A. García, F. Plazaola, V. Muñoz-Sanjosé, and C. Martínez-Tomás, "Near band edge recombination mechanisms in GaTe," Phys. Rev. B **68**(24), 245202 (2003).
16. Q. Zhao, T. Wang, Y. Miao, F. Ma, Y. Xie, X. Ma, Y. Gu, J. Li, J. He, B. Chen, S. Xi, L. Xu, H. Zhen, Z. Yin, J. Li, J. Ren, and W. Jie, "Thickness-induced structural phase transformation of layered gallium telluride," Phys. Chem. Chem. Phys. **18**(28), 18719–18726 (2016).
17. L. C. Muhimmah and C.-H. Ho, "Dual phase two-color emission observed in van der waals GaTe planes," Appl. Surf. Sci. **542**, 148593 (2021).
18. C. H. Ho, C. C. Wu, and Z. H. Cheng, "Crystal structure and electronic structure of $GaSe_{1-x}S_x$ series layered solids," J. Cryst. Growth **279**(3-4), 321–328 (2005).
19. C. H. Ho, M. C. Chiou, and T. M. Herninda, "Nanowire grid polarization and polarized excitonic emission observed in multilayer GaTe," J. Phys. Chem. Lett. **11**(3), 608–617 (2020).
20. K. C. Mandal, R. M. Krishna, T. C. Hayes, P. G. Muzykov, S. Das, T. S. Sudarshan, and S. Ma, "Layered GaTe crystals for radiation detectors," IEEE Trans. Nucl. Sci. **58**(4), 1981–1986 (2011).
21. K. C. Mandal, S. Das, R. Krishna, P. G. Muzykov, S. Ma, and F. Zhao, "Surface passivation of p-GaTe layered crystals for improved p-GaTe/n-InSe heterojunction solar cells," *Mater. Res. Soc. Symp. Proc.* 1268, EE02 (2011).
22. C. J. Bae, J. McMahon, H. Detz, G. Strasser, J. Park, E. Einarsson, and D. B. Eason, "Influence of thickness on crystallinity in wafer-scale GaTe nanolayers grown by molecular beam epitaxy," AIP Adv. **7**(3), 035113 (2017).
23. H. Cai, J. Kang, H. Sahin, B. Chen, A. Suslu, K. Wu, F. Peeters, X. Meng, and S. Tongay, "Exciton pumping across type-I gallium chalcogenide heterojunctions," Nanotechnology **27**(6), 065203 (2016).
24. J. J. Fonseca, S. Tongay, M. Topsakal, A. R. Chew, A. J. Lin, C. Ko, A. V. Luce, A. Salleo, J. Wu, and O. D. Dubon, "Bandgap restructuring of the layered semiconductor gallium telluride in air," Adv. Mater. **28**(30), 6465–6470 (2016).
25. K. F. Mak, K. He, C. Lee, G. H. Lee, J. Hone, T. F. Heinz, and J. Shan, "Tightly bound trions in monolayer MoS_2," Nat. Mater. **12**(3), 207–211 (2013).
26. S. Mouri, Y. Miyauchi, and K. Matsuda, "Tunable photoluminescence of monolayer MoS_2 via chemical doping," Nano Lett. **13**(12), 5944–5948 (2013).
27. K. Xiao, T. Yan, and X. Cui, "Dipole orientation shift of ga2se2 by quantum confinement," ACS Nano **14**(1), 1027–1032 (2020).
28. A. Zubiaga, J. A. Garcia, F. Plazaola, V. Munoz-Sanjose, and M. C. Martinez-Tomas, "Recombination processes in unintentionally doped gate single crystals," J. Appl. Phys. **92**(12), 7330–7336 (2002).
29. Y. Cui, D. D. Caudel, P. Bhattacharya, A. Burger, K. C. Mandal, D. Johnstone, and S. A. Payne, "Deep levels in GaTe and GaTe:In crystals investigated by deep-level transient spectroscopy and photoluminescence," J. Appl. Phys. **105**(5), 053709 (2009).
30. O. Salehzadeh, N. H. Tran, X. Liu, I. Shih, and Z. Mi, "Exciton kinetics, quantum efficiency, and efficiency droop of monolayer MoS_2 light-emitting devices," Nano Lett. **14**(7), 4125–4130 (2014).
31. L. Yuan, T. Wang, T. Zhu, M. W. Zhou, and L. B. Huang, "Exciton dynamics, transport, and annihilation in atomically thin two-dimensional semiconductors," J. Phys. Chem. Lett. **8**(14), 3371–3379 (2017).
32. L. Yuan and L. B. Huang, "Exciton dynamics and annihilation in WS_2 2D semiconductors," Nanoscale **7**(16), 7402–7408 (2015).
33. D. Z. Sun, Y. Rao, G. A. Reider, G. G. Chen, Y. M. You, L. Brezin, A. R. Harutyunyan, and T. F. Heinz, "Observation of rapid exciton-exciton annihilation in monolayer molybdenum disulfide," Nano Lett. **14**(10), 5625–5629 (2014).
34. X. Fan, W. Zheng, H. Liu, X. Zhuang, P. Fan, Y. Gong, H. Li, X. Wu, Y. Jiang, X. Zhu, Q. Zhang, H. Zhou, W. Hu, X. Wang, X. Duan, and A. Pan, "Nonlinear photoluminescence in monolayer WS_2: Parabolic emission and excitation fluence-dependent recombination dynamics," Nanoscale **9**(21), 7235–7241 (2017).